STAFF SUMMARY SHEET

	TO	ACTION	SIGNATURE (Surname), GRADE AND DATE		TO	ACTION	SIGNATURE (Surname), GRADE AND DATE
1	DFAN	sig	James K. Hall	6			
2	DFER	approve	Kraus, Col 12 JUN 13	7			
3	DFAN	action	(Author /Originator)	8			
4				9			
5				10			

SURNAME OF ACTION OFFICER AND GRADE	SYMBOL	PHONE	TYPIST'S INITIALS	SUSPENSE DATE
Chrs Porter		333-9405	cp	20130617

SUBJECT		DATE
Clearance for Material for Public Release	USAFA-DF-PA- 383	20130611

SUMMARY

1. PURPOSE. To provide security and policy review on the document at Tab 1 prior to release to the public.

2. BACKGROUND.
Authors: Chris Porter, Jurgen Seidel, Robert Decker, and Thomas McLaughlin

Title: Numerical Simulations of Aero-Optical Distortions Around Various Turret Geometries

Circle one: Abstract (Tech Report) Journal Article Speech Paper Presentation Poster
Thesis/Dissertation Book Other: _____

Check all that apply (For Communications Purposes):
[] CRADA (Cooperative Research and Development Agreement) exists
[] Photo/ Video Opportunities [] STEM-outreach Related [] New Invention/ Discovery/ Patent

Description: Numerical simulations around various optical turret geometries are investigated to determine their effect on resulting optical aberrations of a collimated beam propagating through the flow field. An adaptive optic approach is used to mitigate these aberrations by estimating their shape and magnitude based on surface presure measuremnts and OPD-POD modes.

Release Information: To be submitted to the HPCMP DoD Mission Success Story Proceedings to highlight how HPC is used by the DOD science comunnity to support DoD's mission-critical requierements.

Previous Clearance information: (If applicable): If another agency has endorsed the release, say so here. State who sponsored the work.

Recommended Distribution Statement: Distribution A: approved for public release, distribution unlimited

3. DISCUSSION.

4. RECOMMENDATION. Sign coord block above indicating document is suitable for public release. Suitability is based solely on the document being unclassified, not jeopardizing DoD interests, and accurately portraying official policy.

Thomas E. McLaughlin, Ph.D.
Director, Aeronautics Research Center

Numerical Simulations of Aero-Optical Distortions Around Various Turret Geometries

Chris Porter, Jürgen Seidel, Robert Decker, and Thomas McLaughlin
Department of Aeronautics, U.S. Air Force Academy
USAF Academy, CO 80840

Abstract

At compressible flow speeds, the flow around blunt objects such as optical turrets creates time- and spatially-varying density fields. These inhomogeneous density fields mean that an inhomogeneous index-of-refraction field exists around the optical-turret. As a result, as light traverses through this field, an otherwise collimated wavefront becomes distorted. These distortions reduce the farfield irradiance that can be delivered on a target. In an effort to understand and mitigate these flow-induced optical aberrations, numerical simulations of the Navier-Stokes equations were performed on various turret geometries. The results indicate that minor changes in geometry, such as the addition of a flat optical window, can have a large effect on the system performance. To mitigate these problems, numerical decompositions of the optical aberrations at various viewing angles were performed and related to measurable quantities such as the pressure around the aperture. Surface pressure measurements allowed for using adaptive-optics to correct these aberrations. The results indicate that through these techniques the farfield irradiance delivered on target is almost restored back to the diffraction-limited case.

I. Aero-Optics Problem Description

Lasers and other optical instrumentation are now routinely mounted on aircraft for a variety of applications such as optical communications and directed energy. For these applications, it is critically important for the successful operation of the system to maintain a tightly focused spot on a target. For a given optical system, the ability to focus a beam of light on a target is impaired by optical aberrations caused by the air between the laser and the target. In particular, as light travels through an inhomogeneous index-of-refraction field, aberrations are imprinted onto the wavefront as regions of the beam speed up or slow down, resulting in a non-planar wavefront. These aberrations degrade the ability to focus the beam on a target.

For a fluid, the Gladstone-Dale relation links density variations to the index-of-refraction field,

$$n\left(\vec{x},t\right) = 1 + K_{GD}\rho\left(\vec{x},t\right). \tag{1}$$

One source of density variation is temperature fluctuations associated with atmospheric turbulence [1]. This atmospheric-optics problem is relatively well understood since it affects different applications ranging from astronomical observations to aerial imaging and tracking. On the other hand, density variations are also created by the turbulent, compressible flow around an aircraft in flight [2, 3]. These aircraft-generated flow fields generate optical aberrations which are referred to as "aero-optic" aberrations. In general, aero-optics is a less-mature field compared to atmospheric-optics. Furthermore, aero-optic flows are typically more challenging than atmospheric-optics flows due to the higher aberration magnitudes, the much higher frequencies, and the concomitant smaller spatial scales. The problem is further complicated by vortex-induced vibrations, resulting from the fluid-structure interaction between the air and the turret, which leads to beam jitter where the beam can not be focused steadily in one spot [4–6].

Over the past several decades, the wavelength of the lasers used in airborne applications has been reduced to deliver a larger irradiance to a target. A consequence of reducing the laser's wavelength was that the effects of the compressible flow near the aircraft became significantly more important. In particular, while the hemispherical turret provides an efficient means for directed energy to enter or exit the aircraft and enable the beam to track over a significant range of elevation and azimuth angles, the turret causes the flow to separate, creating an optically active wake. These optical effects cannot be ignored. As a result of the optically active wake, the current conclusion of research into these aero-optic effects is to limit the realistic field-of-regard of high-energy laser systems to forward-looking angles. For instance, a 1 μrad deflection in the optical wavefront (e.g. tip/tilt) results in the centroid of the beam displacing 2 meters at a distance of 200 kilometers away from the turret.

To quantify the aero-optics problem, two general metrics are typically used: (1) the OPD_{RMS} and (2) the Strehl ratio (SR). The OPD_{RMS} is used to quantify the near-field optical effects of an inhomogeneous index-of-refraction

field, based on the optical path difference (OPD):

$$OPD\left(\vec{x},t\right) = OPL\left(\vec{x},t\right) - \overline{OPL}\left(\vec{x},t\right), \tag{2}$$

where the optical path length (OPL) is defined as

$$OPL\left(\vec{x},t\right) = \int_{s1}^{s2} n\left(\vec{x},t\right) dx. \tag{3}$$

Under certain conditions [7], the spatial root-mean-square (RMS) of the OPD can be used in conjunction with the Marchél approximation to estimate the Strehl ratio,

$$SR(t) = \frac{I}{I_0} = \exp\left(-\left[\frac{2\pi OPD_{RMS}(t)}{\lambda}\right]^2\right) \tag{4}$$

which defines the *on-axis* farfield irradiance to the *on-axis* diffraction-limited farfield irradiance. Note that when this version of the Strehl ratio is used, optical jitter and tip/tilt effects have been removed. In the next section, computational results are used to examine the aero-optics problem and a methodology is presented to estimate these aberrations and correct for them in real time.

II. Numerical Method

The CFD simulations were performed using COBALT V5.2 from Cobalt Solutions, LLC, an unstructured finite-volume code developed for the solution of the compressible Navier-Stokes equations. The basic algorithm is described in Strang et al. [8], although substantial improvements have been made since then. The numerical method is a cell-centered finite volume approach applicable to arbitrary cell topologies. The spatial operator uses the exact Riemann Solver of Gottlieb and Groth, least squares gradient calculations using QR factorization to provide second order accuracy in space, and TVD flux limiters to limit extremes at cell faces [9]. A point implicit method using analytic first-order Jacobians is used for advancement of the discretized system. For time-accurate computations, a second-order accurate method with five Newton sub-iterations is employed. Delayed Detached-Eddy Simulation (DDES) with a SST turbulence model is used for all the simulations to compare the effects of the different geometries.

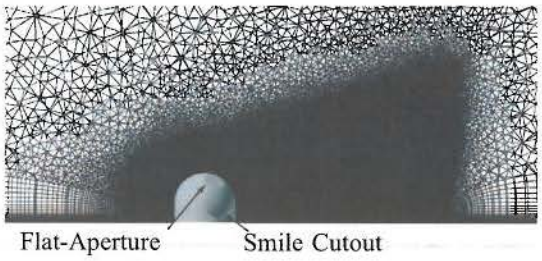

Fig. 1. Flat window turret with smile geometry and grid.

A. Computational Domain and Setup

The basic geometry under consideration is a three-dimensional turret. The base cylinder has a diameter of D = 30.5 cm and is H_{cyl} = 10 cm tall. The diameter of the optical aperture is A_D = 10 cm , and for the flat-window turret, the flat has a diameter of A_D = 10.5 cm to allow for the introduction of pressure sensors and/or actuators around the aperture, and is orientated at an 50° elevation angle. For the two geometries with "smile" cutouts, the cutouts and aperture are oriented at an azimuthal angle of 120°. The basic smile geometry implemented is identical to the geometry used in Notre Dame's Airborne Aero-Optics Laboratory [3]. Figure 1 shows a slice though the grid of the turret with a flat-window and smile geometry. Note that grid structure shown in Fig. 1 is representative of the grid used in the other three geometries simulated.

The SimCenter software suite was used to generate the computational domain and grids. The turret was surrounded by a refinement region that extended x/D = 1 upstream and laterally of the turret and x/D = 3 downstream to capture the recirculation region behind the turret. The coordinate system is oriented such that the x-axis points downstream, the y-axis vertically up, and the z-axis is in the spanwise direction. The inflow boundary is x/D = 7.5 upstream of the turret, while the downstream boundary is x/D = 15 downstream to allow fluidic structures to dissipate before reaching the boundary. In the y- and z-directions, the grid extends to y/D = 7.5 and z/D = 15 to allow for sufficient distance to the boundary to minimize reflections. The grid spacing on the turret was ds = 1 mm on the turret surface and $dn = 2\times10^{-4}$ mm in the wall normal direction, which resulted in an average $y+ < 1$. Spacing around the flat-window as well as the smiles was further refined to help capture the sharp geometrical changes on the turret. Table I lists the total number of cells for each geometry, along with the viewing angles at which optical properties are calculated. Note that two of the grids have two total cell numbers listed to verify spatial convergence. The time step for each calculation was held constant at $\Delta t = 5 \times10^{-6}$ s, which

Geometry	Number of Cells	CFL	Beam azimuth angles (°)	Beam elevation angles (°)
Conformal-window	70M/125M	4	45,90,120,150,180	45,50,50,50,50
Flat-window	70M/125M	4	120	50
Conformal-window w/smile	168M	4	120,120,120,120,120	0,25,50,90,135
Flat-window w/smile	162M	4	120	50

TABLE I. GRID SIZE AND BEAM LOCATIONS FOR THE FOUR DIFFERENT TURRET GEOMETRIES SIMULATED.

provided an average CFL number of ~4 for the finest grid to ensure temporal accuracy. The inflow Mach number was maintained at Ma=0.4. Standard atmospheric conditions at an altitude of 4,572 m were prescribed at the inflow to match flight experiments conducted by the University of Notre Dame. [3, 4] The resulting Reynolds number, based on the turret diameter, is approximately Re=900,000.

To study the optical properties of the flow field, the flow field data were written out on beam grids (created using Cobalt's tap feature) and analyzed using Eqs. (1)-(2). Depending on the geometry tested, different tap grids were required. For instance, on the canonical conformal-window turret, five different tap grids could be applied in a single computation. In this case, various azimuthal angles of interest were used to study optical effect in different flow regimes. For the conformal turret with the smile geometry, five beam tap grids were also used. However, in this case, the azimuth angle was limited to 120° and the elevation angle was altered. For the flat window turret, the tap grid is fixed to the flat aperture and separate simulations are necessary for different viewing angles.

Compute times, including the data input/output (I/O), were measured at approximately 92 CPUs/iteration or 1.3s/cell/iteration for the two largest grid used. the simulations were calculated using 512 cpus for a total of 7000 time steps including the numerical startup.

III. RESULTS

All four turret geometries were simulated under the conditions mentioned above to compare both the changes in the flowfield and resulting optical aberration imprinted onto an otherwise collimated beam. Figure 2 shows instantaneous density fluctuations ($\rho' = \rho - \overline{\rho}$) around the two turret configurations without the "smile" cutouts. In Figure 2, two different slices through the flow field are shown, one along the centerline of the turret, and the other through the center of the aperture. In all the figures showing ρ' throughout this document, the colormap has been held constant for direct comparison.

For the conformal-windowed turret, the presence of the two horn vortices creates a large downwash, causing the shear layer to stay close to the turret surface. At the aperture plane, which cuts through one of the horn vortices, the induced downwash is not as prevalent and the shear layer forms much farther away from the turrets surface. In both cases however, the formation of a Kelvin-Helmholtz type shear layer is not seen. When the flat-aperture is added, a fixed separation point exists due to the surface discontinuity. This creates an asymmetry in the flow field and reduces the local downwash created by the horn vortex on the side of the aperture. In both slices of the flat-aperture, the shear layer that forms is all but parallel to the floor, creating a much larger wake and therefore pressure drag on the turret. This forced separation also creates the necessary conditions for the formation of a Kelvin-Helmholtz type shear layer, causing coherent vortical structures with reduced pressure and density to form. The overall result is a much more severe aero-optic environment.

To see the effect that the "smile" cutouts in the optical turret have on the flow, additional simulations were performed on the two remaining turret geometries. Figure 3 shows the mean removed density for these geometries along the same slices shown in Figure 2. The additional cut-outs created large vortical structures forming along the cylindrical base of the turret (see Figure 4). This widened the overall wake of the turret and reduced the coherence of the two horn vortices. As a result, the wake of the turret is much larger than its geometric counterpart without the "smiles." In these cases, the "smile" cutouts create both a forward- and backward-facing step on the port and starboard sides of the turret. On the starboard side, the flow separates and forms a Kelvin-Helmholtz type shear layer at the backward-facing step, whereas the forward-facing step is fully engulfed in the turret's wake. On the port side, the flow separates at the backward-facing step created by the cutout but quickly reattaches creating a closed separation bubble within the cutout. After reattaching, the flow then experiences a forward facing step where it once again separates forming another open shear layer. The result of these cutouts is a large asymmetry in the overall flow field. Finally, both of these shear layers cause a widening of the wake and interact with the formation of the two horn vortices. This interaction propagates all the way up the turret and in fact alters the flow over the aperture of the turret.

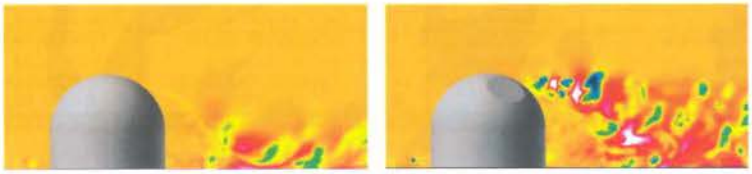

(a) Conformal window - center plane (b) Flat window - center plane

(c) Conformal window - aperture plane (d) Flat window - aperture plane

Fig. 2. Mean-removed density (ρ') contours at Mach 0.4 for a conformal- and flat-windowed turret.

(a) Conformal window w/smile - center plane (b) Conformal window w/smile - aperture plane

(c) Flat window w/smile - center plane (d) Flat window w/smile - aperture plane

Fig. 3. Mean-removed density (ρ') contours at Mach 0.4 for a conformal- and flat-windowed turret with "smile" cut-outs.

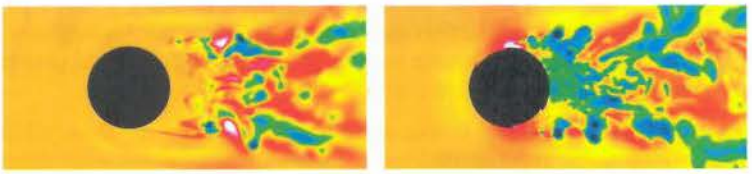

(a) Conformal window (b) Conformal window w/smile

(c) Flat window (d) Flat window w/smile

Fig. 4. Mean-removed density (ρ') contours at Mach 0.4 5 cm above the floor (through the center of the "smile" cutouts if present).

Once the flow field around each turret was calculated, the resulting aberrations of an otherwise collimated beam were calculated as it propagates through the flow. To correct for these aberrations, a feedback system based on various numerical decomposition techniques was initiated. As a first step, the OPD data (static-lensing and tip/tilt

removed) for each beam as a function of time was decomposed using Proper Orthogonal Decomposition (POD) [10]. Using POD, the OPD data is decoupled spatially and temporally. An example of the POD spatial modes is shown in Fig. 5 for the conformal-window OPD at an Az = 120° and El = 50°. Note that in the beam reference frame, the bottom left corner of each of the figures corresponds to the downstream edge of the aperture, while the upper right corresponds to the upstream edge of the aperture.

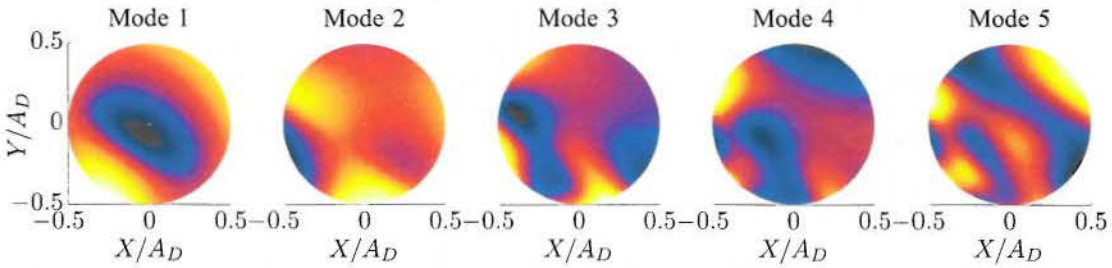

Fig. 5. Calculated OPD (static-lensing and tip/tilt removed) POD spatial modes for an azimuth angle of 120° and an elevation angle of 50° on the conformal-window turret.

Once the OPD data was decomposed into spatial and temporal modes, the corresponding time coefficients for a given set of spatial modes provides an estimate of what the instantaneous OPD is without directly measuring it. Therefore, pressure sensors (using surface tap data in the simulations) were placed around the aperture to correlate the OPD POD time coefficients to the measured pressure signals. As a first step, 20 pressure sensors were placed 0.4 cm from the edge of the aperture; the pressure sensors were equally spaced circumferentially around the aperture. Using the pressure signals around the aperture, a linear mapping was used to correlate the pressure to the POD time coefficients for each beam:

$$a_i(t) = C * P_s. \tag{5}$$

To develop the mapping matrix, C, the first 150 ($\tau = tU_\infty/D = 1.57$) data points were used. With the resultant mapping matrix, the OPD for the remaining time steps was estimated based only on the pressure measured on the surface of the turret. Figure 6 shows the calculated $\mathrm{OPD_{Norm}} = OPD_{RMS}/\rho M^2 D$ as a function of τ for beam angles of Az = 90° and Az = 120°. In Fig. 6, the corrected signal is obtained by removing the predicted OPD from the actual OPD. To obtain the predicted OPD, the estimated time coefficients (Eq. (5)) were multiplied by the corresponding spatial modes (φ) and summed,

$$\widehat{OPD} = \sum_{i=1}^{n=20} a_i \varphi_i, \tag{6}$$

where the hat denotes the estimated OPD. As shown in Fig. 6, this technique was able to reduce the $\mathrm{OPD_{Norm}}$ substantially during the training session (left of the vertical dotted line), and even reduced the $\mathrm{OPD_{Norm}}$ during the predicted region (right of the dotted vertical line) by at least 50 percent.

In the data above, very few flow cycles were used to estimate C. To provide a larger data sample to train the mapping matrix, C, several additional simulations were performed. Due to the computational expense, continuing the current simulations with such a small time step was prohibitive. Therefore, the time step in the simulation was increased to a corresponding average CFL number of approximately 30, at the expense of increased temporal errors. Given the increased error, the goal of this part of the investigation was to show that increasing the amount of data available for training will further increase the performance of this technique by providing a better estimate of the training matrix, C. The results indicated that while the OPD_{NORM} values changed slightly, due to temporal errors, the method was able to predict the actual OPD_{NORM} very accurately, and the additional training data greatly aided in the training of the C matrix. This technique was applied to the other turret geometries with similar results. As a final verification of the method, simulations were performed using different turbulence models, or even none at all, and while the wavefront abberations changed drastically, indicating the sensitivity of the calculations, estimating the OPD based on POD worked in all cases. In fact, in some instances, this method was able to capture all but 0.1 percent of the actual OPD. The end result is that the resulting Strehl ratio was greatly increased indicating a drastic improvement in the overall system performance.

IV. Conclusions

In this paper, the flow field around four different optical turrets was analyzed for the aero-optical implications of typical geometry modifications to a canonical turret. Using High Performance Computing Modernization Program

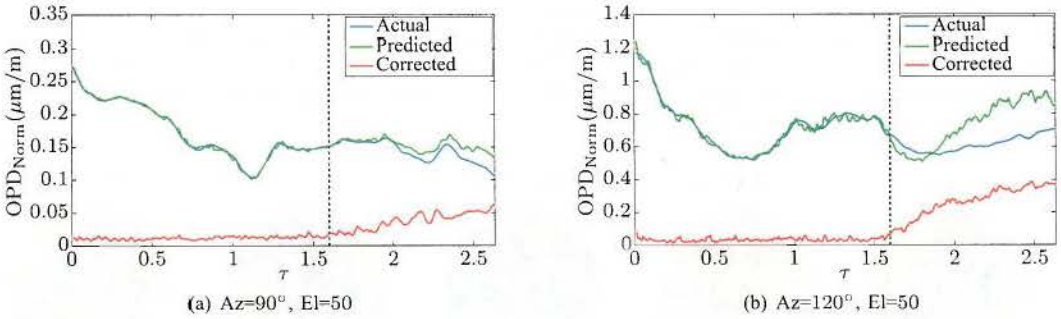

(a) Az=90°, El=50 (b) Az=120°, El=50

Fig. 6. Actual and predicted OPD_{Norm} values.

(HPCMP) resources under the Challenge Project C4L, Delayed Detached-Eddy Simulations using Cobalt were performed to study the flow-field. Optical analysis of the simulation results show significant beam distortions for all viewing angles under consideration. Using numerical decomposition techniques and surface pressure measurements, these optical distortions can be predicted and an adaptive optics system was successfully employed to counter these aero-optical effects. This resulted in at least a 50 percent reduction in the OPD_{RMS} and in some instances almost eliminated the whole wavefront distortion. The end result is a drastic increase in the Strehl ratio, and a overall increase in system performance.

V. Acknowledgements

The DoD HPCMP supported this project by supplying supercomputer time under Challenge Project C4L at the DoD Distributed Resource Center at Maui, Mississippi, and Alaska.

The material is based on research sponsored by the US Air Force Academy under agreement number FA7000-10-2-0026. The U.S. Government is authorized to reproduce and distribute reprints for Governmental purposes notwithstanding any copyright notation thereon.

The views and conclusions contained herein are those of the authors and should not be interpreted as necessarily representing the official policies and endorsements, either expressed or implied, of the U.S. Air Force or the Government.

References

[1] V. L. Tatarskii and V. U. Zavorotnyi, "Wave propagation in random media with fluctuating turbulent parameters," *J. Opt Soc Am A*, vol. 2, no. 12, pp. 2069–2076, 1985.

[2] E. J. Jumper and E. J. Fitzgerald, "Recent advances in aero-optics," *Prog. Aero. Sci.*, vol. 37, pp. 299–339, 2001.

[3] C. Porter, S. Gordeyev, M. Zenk, and E. Jumper, "Flight measurements of aero-optical distortions from a flat-windowed turret on the airborne aero-optics laboratory (aaol)," in *AIAA Paper 2011-3280*, 2011.

[4] N. D. Lucca, S. Gordeyev, and E. J. Jumper, "The airborne aero-optics laboratory, recent data," *Acquisition, Tracking, Pointing, and Laser Systems Technologies XXVI. Proceedings of SPIE*, vol. 8395, 2012.

[5] N. D. Lucca, S. Gordeyev, and E. Jumper, "The study of aero-optical and mechanical jitter for flat window turrets," in *AIAA Paper 2012-0623*, 2012.

[6] Z. Ponder, S. Gordeyev, E. Jumper, S. Griffin, and C. McGaha, "Passive mitigation of aero-induced mechanical jitter of flat-windowed turrets," in *AIAA 2011-3281*, 2011.

[7] C. Porter, S. Gordeyev, and E. Jumper, "Large-aperture approximation for not-so-large apertures," *Optical Engineering*, vol. 52, March 2013.

[8] W. Strang, R. Tomaro, and M. Grismer, "The Defining Methods of Cobalt60: A Parallel, Implicit, Unstructured Euler/Navier-Stokes Flow Solver," in *AIAA Paper 1999-0786*, 1999.

[9] J. J. Gottlieb and C. P. T. Groth, "Assessment of Riemann Solvers for Unsteady One- Dimensional Inviscid Flows of Perfect Gases," *J. Comp. Phys.*, vol. 78, pp. 437–458, 1988.

[10] P. J. Schmid, K. E. Meyer, and O. Pust, "Dynamic mode decomposition and proper orthogonal decomposition of flow in a lid-driven cylindrical cavity," in *8TH INTERNATIONAL SYMPOSIUM ON PARTICLE IMAGE VELOCIMETRY - PIV09*, August 25-28, 2009.